Pre-clinical radiotherapy

CHAPTER 7

Summary, discussion, and prospective work

7.1 Summary and discussion

The rise of small-animal image-guided precision radiotherapy platforms has been revolutionizing translational and radiobiological research. Modern devices and current advanced tumour models have enabled fundamental research on irradiation protocols, fractionation regimens, adjuvant therapies and established concepts in controlled environments, with large (transgenic) animal cohorts and accelerated results. A number of biological, physical and technological concerns remain. A recent report from the European society for radiotherapy and oncology advisory committee in radiation oncology practice (ESTRO ACROP) numbered the main challenges to be addressed in this field[1]; it enquires about:

- the key technologies for downscaling clinical treatments and the imaging modalities to be integrated and potentially used in treatment planning;
- the treatment of target motion and optimal irradiation margins;
- the accuracy and precision of small field dosimetry and dose distribution verification;
- the difference between high and low-energy photon irradiation.

Although categorized into different topics, the challenges have a synergetic relationship: imaging requires sub-millimetric resolution, affects dosimetry and is affected by motion; and pre-clinically mimicking clinical scenarios requires lower energies to avoid large beam penumbras and dose (re-)buildup regions which also affect dosimetry and might yield different treatment outcomes if dose calculations do not consider medium heterogeneities.

This thesis has briefly introduced the historical evolution of radiotherapy and the need for pre-clinical EBRT research **(Chapter 1)**. It presented ways to tackle some of these challenges and warned about their drawbacks. In the following sections, the research concerning these and additional points is summarized, discussed and future perspectives from discussion points are canvassed.

7.1.1 Imaging and dose calculations

In a framework to establish imaging protocols that allow accurate dose calculations, Chapter 2 examined the feasibility of using dual energy CT (DECT) to extract tissue atomic compositions and assess dose calculation accuracy gain. The study demonstrated improved accuracy for DECT in comparison to SECT. It stressed the arbitrariness of the broadly used SECT method: it is not clear which media and how many linear segments should be used for generating a calibration curve, and where to place material boundaries. The latter are often selected based on visual inspection, yielding inter-individual differences. In this study, three main debatable topics were analysed: tissue compositions, energy dependence and image quality.

Segmenting a specimen using only a single dense bone material with elevated effective atomic number caused high absorption, resulted in less photoelectric interactions in soft tissue, higher dose deposition in osseous tissues and underestimation in the organs at risk (OARs) in proximity of bone. On the other hand, the choice of multiple bone types, using DECT, resulted in lower dose values for the different tissues occupying the same volume and minimal assignment of (human) cortical bone (1.9%). It was recommended to segment mice using bony tissues with decreased density and effective atomic number values considering that their bones are flexible and possibly closer to human cartilage in composition. Additionally, incorrect material segmentation was shown to be aggravated with a decrease in beam energy due to the intensified role of photoelectric cross-sections, causing materials with different effective atomic numbers to absorb increasingly different fractions of energy. These two subjects, energy dependence and tissue compositions, are echoed throughout this thesis and have a deterministic relationship in this field.

Although necessary for MC dose calculations, tissue compositions have a marginal impact on clinical EBRT photon treatments, where incoherent interactions are predominant and dependent on tissue electron density[2]. Their influence is higher on clinical proton EBRT and kV techniques such as brachytherapy and small animal radiotherapy. For clinical protons beams, they influence the mean excitation energy used to calculate the proton stopping power ratio and affect range verification techniques. For kV techniques, although Compton interactions are still important, photoelectric probability is significant and this effect is strongly dependent on the atomic number of the medium (Z^{3-4}). The mass-energy absorption

coefficients, a quantity closely related to absorbed dose, may differ by more than a factor of six for low energies[3].

The assignment of tissue compositions is a bottleneck in radiotherapy. In pre-clinical EBRT, human tissue compositions are predominantly used due to the scarce literature on animal ones. A small number of studies has presented quantitative data on animal tissues[4-9], albeit unspecific for radiotherapy or focused on trace-elements. The increased biological interest on molecular or cellular entities rather than atomic ones and the practical difficulties in establishing atomic compositions are possible culprits. Clinical radiotherapy uses human tissue reference data listed in reports 46 of the International Commission on Radiation Units and Measurements (ICRU) and report 23 from the International Commission on Radiological Protection (ICRP) [10-12].

Mann-Krzisnik has published a thorough study, which describes how the human reference data was established[13]. It reports that measurements were taken between 1940 and 1960. Lighter elemental composition (hydrogen, carbon, nitrogen and oxygen) was extrapolated from gross proportions of water, fat, proteins and carbohydrates while heavier elements were derived from spectrographic analysis of ashed and dried tissue samples extracted from cadavers. A number of issues was observed, e.g. some tissue compositions did not sum up to 100% or did not contain carbon, which is considered impossible for a biological tissue. Data was later rendered by several sources and renormalized, which may have added inconsistencies as individual studies started from different premises (e.g. distinct levels of hydration or manipulation methods). Additionally, lighter elemental composition derivations may have neglected variations in chemical composition of fats, proteins and carbohydrates and the method employed for heavier elements possibly lacked precision. All measurements were derived from ex vivo samples, which might differ from in vivo ones in terms of tissue compositions, hydration and densities. Moreover, akin to elemental composition, ICRU and ICRP density reference data is connected to the same studies, rendered from several publications and prone to similar issues. Different from elemental compositions, density is typically derived from CT scans rather than reference data, hence the importance of this reference parameter is decreased.

Dosimetric implications of using human tissue compositions in mice have been investigated with DECT and differences between human and

murine elemental compositions led to dose errors of up to 20.1% for bones in addition to a large spread in mass-energy absorption coefficients for different tissues[14]. These results stress the need of research on reference data or, minimally, establishing a relationship between human and animal tissues; for murine studies (and for other specimens used for radiotherapy research), population samples should include different strains, genders and ages as concentration of certain elements vary within these categories. Moreover, the large spreads indicate that assigning one mean reference value to a whole organ is not realistic as there is a distribution of compositions. New technologies should be explored to derive updated quantities both in invasive and non-invasive ways. This topic is revisited in section 7.2.1.

Finally, Chapter 1 raised an image quality discussion motivated by extensive artefacts and noise on the CT scans. For the former, partial volume effects can explain the high source of errors on the boundary regions. For the latter, rather than uniform, the bulk of the phantom displayed a texture-like appearance, with irregular CT numbers (42±62 and 16±57 HU for 50 and 90 kVp scans) possibly due to noise; moreover the DECT material image, effective atomic number (Z_{eff}) image, was noisy and presented a mean Z_{eff}-value encompassing several soft tissues (mean of 8.0±0.4, ranging from 6.0 to 10.7). As the CT projections were reconstructed with a simple Feldkamp-Davis-Kress (FDK) back-projection algorithm, it was presumed that the usage of iterative reconstruction algorithms with artefact correction kernels could improve the effect of noise and provide superior DECT material segmentation.

7.1.2 Iterative methods for image reconstruction

To analyse the effect of different image reconstruction techniques on image quality and DECT metrics, Chapter 3 presented a software platform for pre-clinical CBCT image reconstruction. Pre-processed projections were reconstructed using the analytical filtered back-projection (FDK) or the iterative reconstruction (IR) algorithms, e.g. iterative FDK, simultaneous algebraic reconstruction technique (SART), simultaneous iterative reconstruction technique (SIRT) or Conjugate Gradient (CG). A cupping correction was included, a polynomial pre-correction to the attenuation data for linearization. Imaging metrics were quantitatively assessed with a quality assurance phantom and DECT analysis was performed to determine the influence of each reconstruction technique on the relative electron density (ρ_e) and Z_{eff} values.

IR methods proved computationally costly due to the large matrices and small pixel sizes chosen for the study but presented satisfactory results with smaller grids, typical of pre-clinical practice. Nevertheless, reconstruction times were longer when compared to analytical methods as these algorithms use multiple repetitions. With increased computational power and the use of graphical processing units (GPUs), both with current technology, this difference can become negligible and not represent a limiting factor for online iterative reconstruction: time is of the essence in this field as animals are imaged while restrained under sedation and long anaesthesia times might impair the fitness of the specimen and the integrity of the study; this topic is further discussed in section 7.2.2.

The cupping artefact correction provided accurate CT numbers and could benefit larger subjects and applications that require increased image accuracy. The workflow needs improvement, as reconstructing an object a number of times to derive a polynomial, which will correct a final reconstruction, is a lengthy and impractical process. Either a fixed polynomial order could be chosen in advance according to the object size or different algorithms could be applied. Regarding DECT, IR showed significantly smaller spread for each material in the ρ_e-Z_{eff} space and lower Z_{eff} and ρ_e residuals (on average 24% and 25% lower, respectively). This is an important result as it indicates that imaging noise was reduced and the IR methods provided tissue composition distributions closer to the reference values. Thus, IR could benefit DECT tissue segmentation as the spread in ρ_e-Z_{eff} space could be closer to the spread in tissue values, and less affected by errors intrinsic to the imaging modality. A myriad of iterative methods exists and provide different degrees of accuracy and computational times. This study showed the development of the software and a first application to small animal CBCT. Other algorithms, and back-projection, forward-projection and window type filters, already foreseen in the software, should be further characterized and additional artefact kernels further implemented to expand the reach of these techniques.

Considering the image quality aspect, the analysed reconstruction techniques provided acceptable and similar geometric accuracy, uniformity and CT number results. SART provided improved contrast-to-noise ratio (CNR) but lower resolution for some media, when compared to the other techniques. Accuracy on image metrics is crucial for dose calculations, as the contours of anatomical structures can suffer from reduced resolution, abundance of noise or non-uniformity. Geometric accuracy and contrast

are also important for spatial targeting and measurements of anatomical structures, which can determine how a tumour or an OAR is responding to treatment. The influence of the scanning parameters in terms of current, frame rate, rotational speed, gain and exposure were adopted from established protocols and could be revisited. It would be beneficial to investigate if lower exposure times associated with IR methods would present similar CNR and noise levels at lower imaging doses. High imaging doses from cumulative scans may change the animal immune response and other biological pathways that may alter the experimental outcome[15-17]. Thus, quantification of imaging dose is an important part of system commissioning and operation, especially for longitudinal studies. The use of imaging techniques that provide no radiation dose is also advised, when possible.

Furthermore, an image quality assurance (QA) program should be in effect, following guidelines, which should provide tolerances for normal operation tests, and take corrective actions such as imaging system recalibration if tolerance levels are not met when recommended imaging protocols are used. The QA tests should happen periodically. Currently, due to the lack of specific recommendations, several research institutions have different QA approaches, ranging from extensive tests to the absence of this practice. The 4th Conference on Small Animal Precision Image-Guided Radiotherapy, Lisbon, March 2018, held discussions concerning this topic. Several experts agreed on the need for recommendations and that meanwhile users should design ways to ensure the calibration of their systems. It is possible to find publications with acceptable QA tests[18, 19]. Beyond imaging, the QA program should also include the dosimetry of system, on an annual basis, to estimate the dose rate of the x-ray tube, using an appropriate ionization chamber and correction factors. Following the American Association of Physicists in Medicine (AAPM) Radiation Therapy Committee Task Group 61[20], or similar recommendations[21-23], for reference dosimetry of low- and medium energy x rays for radiotherapy and radiobiology.

7.1.3 Irradiation margins

As mentioned on section 7.1, the treatment of target motion and optimal irradiation margins constitutes a challenge for small animal EBRT. In an attempt to confront these issues, the research presented in Chapter 4 analysed the effect of respiratory motion on irradiation margins for murine lung tumours. Four-dimensional (4D) mathematical phantoms with

different lung tumour locations and extreme breathing curves were used for dose calculations of a 360° arc treatment plan. A time-resolved dose was derived, considering the irradiator gantry rotation and the breathing motion. From different radiotherapy metrics, it was understood that the effect of respiratory motion is dependent on the breathing pattern and the tumour position. Ultimately, a recipe, which considers the irradiation collimator size, was proposed to derive tumour margins and spare OARs by respecting constraints on user-defined metrics. Moreover, the addition of a target margin, especially on sites where movement is substantial, was recommended.

Extreme breathing scenarios were used to represent the possible range where the actual breathing pattern would fall. It varies according to the anaesthesia protocol and the respiratory and cardiac rates. A sedation scenario with minimal motion while physically restraining the specimen is ideal. This study generated a few recommendations to avoid sub-optimal pulmonary treatments. Regarding the orthotopic tumour implantation, when possible, it is recommended to avoid the diaphragm region, as it is the region most affected by motion. Implantations on the superior lobe of the right lung are advised, as the left lung is closer to the heart, an important OAR. The use of motion tracking and gating techniques for imaging and irradiation allow physiological heart and lung motion to have a decreased impact on imaging artefacts and dose heterogeneities [24, 25].

Different gating approaches have been documented and rely on the type of scanner, the specimen and the research in question. In prospective gating, data acquisition is triggered by a motion signal. Prospective methods are used in scanners that operate under step-and-shoot conditions. The x-ray tube is triggered by a user-supplied signal based on the animal physiological motion. Respiratory and cardiac trigger signals can be generated, e.g., with a mechanical ventilator at a selected point in the respiratory cycle, from real-time measurements of a pneumatic cushion positioned on the diaphragm, optical measurements of diaphragm motion, measurements of the heart rate or electrocardiogram (ECG) signal[26-33]. Retrospective gating is performed continuously and all motion correction is applied during post-processing. It can be performed both under continuous rotation or in step-and-shoot mode. Projection images and cardiac and respiratory signals are simultaneously and uninterruptedly recorded. Post-processing includes projection sorting based on the recorded physiological phase of the animal at the time each projection was acquired. Projections acquired in the same

phase are reconstructed[34-36]. Image-based gating determines the portion of the breathing or cardiac cycle in the projection space[37-39]. Different x-ray shutter subsystems have been developed for both commercially available small animal irradiators[40-42], although only one subsystem is in commercial stage. They allow beam gating during treatment, with irradiation only taking place during the breathing cycle when tissue movement is minimal. They facilitate dose delivery during animal movement and are particularly well suited for irradiation of targets within the chest and abdomen. Although not used for the research of Chapter 3, gating techniques contribute to the treatment conformality and are likely to be implemented in most precision irradiators in the near future.

Finally, the use of margins is recommended. This study used a cost function based on dose-volume histogram (DVH) parameters and the available collimators. However, the recipe can be adapted according to adjustable constraints or collimation devices and is independent of the breathing curve; it could be applied for other respiratory or irradiation regimens. A thorough recipe for establishing the concept of planning target volume (PTV) should consider additional parameters such as setup and fractionation errors, when applicable. An important conclusion from this study is the need of considering anatomical and physiological characteristics during clinical to pre-clinical translation, or vice-versa. Although margins are sometimes extrapolated from clinical experience, they might not be representative for certain small animals.

Independently of the margin function, the investigation of an interpolation function for dose accumulation from different anatomic phases to a reference phase using a rigid grid (direct dose mapping) was proposed for speeding up the dose calculation process, as a first approximation: tissue deformation and the cardiac motion were not modelled. Calculation times at least 10 times faster are promising for further development of the technique. However, results may depend on the targeted site and surrounding anatomy. Moreover, as the first time point was considered the reference phase, the dose map derived from the CBCT scan could be subject to noise and blurring. This point was investigated through simulation of the full breathing cycle and effect of respiratory motion on the CT scan blurring was considered minimal while tumour shape was highly preserved. The presented technique could potentially be used for adaptive radiotherapy, which may require the daily delivered dose to be accumulated.

7.1.4 Dose reporting

Another topic highlighted by the ESTRO ACROP report, mentioned in section 7.1, is the treatment (or lack thereof) of different dose reporting quantities generated by the various dose calculation algorithms. Conventional and rather simpler dose calculations methods, which considered the human body as water-equivalent and reported dose to water, have evolved towards sophisticated model-based algorithms e.g. MC. The latter transports radiation through heterogeneous media and report the absorbed dose to a reference medium embedded in a surrounding transport medium. Different dose reporting quantities have been derived using the cavity theory: they are dose-to-medium-in-medium (D_{mm}), dose-to-water-in-medium (D_{wm}) or dose-to-water-in-water (D_{ww}), which acknowledge the dose scoring and the surrounding media as arbitrary or water. These quantities coexist to date and it is debatable which one to favour in detriment of the other. While D_{mm} is more likely to correlate with biological response, clinical experience on tumour, healthy tissue response and dosimetry protocols were built on D_{wm}. Moreover, changing between quantities may yield an additional level of uncertainty.

The study presented in **Chapter 5** analysed the relationship between D_{wm} and D_{mm} on small animal irradiation energies, considering the dependence of D_{wm} with the dose calculation approach using the intermediate cavity theory (ICT). ICT corresponds to a sum of small (SCT) and large (LCT) cavity theory contributions weighted by the parameter d. In other words, it is the weighted sum of electronic stopping power (SCT) and mass-energy coefficient (LCT) ratios between medium and water, $(\overline{S_{el}}/\rho)^{w}_{m}$ and $[\overline{\mu_{en}}/\rho]^{ref}_{m}$. The parameter d was calculated using two different methods, which considered the exponential attenuation of primary electrons as they enter a cavity with secondary particle transmission of 1%[43] or 4%[44]. A set of mathematical phantoms was designed with different voxel sizes, considering the pre-clinical practice and extreme scenarios, and a selection of materials, broad enough to include the range of densities and elemental compositions conventionally used in radiotherapy, as well as an ex vivo mouse chest case with highly heterogeneous regions were included. Local photon spectra were generated in different regions of the chest case. Depending on the energy and the size of the cavity, D_{mm} presented lower or higher values, a factor of 0.68 to 4.37 times D_{wm}.

For soft tissues, except adipose, the relationship between reporting quantities was found equal or close to unity for all different scenarios, an expected behaviour in consequence of the similarities in terms of atomic composition and density amongst the media and water, and small cross section variations. Results for adipose and bony tissues differed as their composition diverges from water. For larger cavities, where the range of secondary particles is smaller or comparable to the cavity dimensions, and for lower energies, where the predominance of photoelectric interactions is increased and highly dependent on the tissue-equivalent material compositions, the difference between dose descriptors was amplified. Hence, the impact of the cavity dimensions on estimated D_{wm} was significant on pre-clinical kilovolt beams up to 225 kVp. Differences up to 5.1% were found between D_{mm}/D_{wm} ratios, calculated using the local spectrum on different regions within the chest case. Therefore, the application of one single conversion factor between quantities for the whole phantom might not be appropriate. Large differences on d values between the two d-deriving methods implied that one should be cautious when using the ICT as there is a lack of consensus on which method to use. Further simulations and measurements, explicitly tracking secondary particles are recommended for establishing a global ICT. The abiding debate over which quantity to favour is foreseen to linger while it is not clear which quantity correlates better with the biological effects of ionizing irradiation; this topic will be revisited in section 7.2.4. Finally, dose distribution comparisons should use the same reporting quantity and caution regarding reported quantity and dose comparisons is advised.

Cavity theory was originally proposed for the determination of absorbed dose in the sensitive volume (a cavity) of a detector, e.g. an ionization chamber. The conversion of absorbed dose in an air-filled cavity to absorbed dose in water was formulated by Bragg in 1912 and Gray in 1936 and later revisited by Spencer, Attix and Burch in 1955 and Nahum in 1978[45-50]. The conditions of the Bragg–Gray (BG) theory with Spencer–Attix–Nahum stopping-power ratios formed the basis of radiation dosimetry protocols widely adopted to MV photon and electron beams[51, 52]. If the dimensions of a cavity are large relative to the range of secondary electrons e.g. for low energy kV beams, the BG conditions do not hold, and the mass-energy absorption coefficient ratios for cavity and medium are normally used. Although several other formalisms were proposed[53-56], including the weighted sum used in Chapter 5, their application remained marginal as treatments with

kV energies are not mainstream and MC methods emerged as a solution to the radiation transport problem allowing accurate estimation of the electron spectra within media. Revisiting this topic, regardless of powerful MC codes that calculate energy deposition in heterogeneous media, has two main justifications. First, not all small animal dose calculation engines use MC models to calculate D_{mm}: some algorithms[57-59] calculate D_{wm} and use conversion factors to D_{mm}. Secondly, besides dose to a water voxel (or a voxel composed of water-like tissue) in medium D_{wm} has been extrapolated to a biological representation of the target where energy is deposited within an organism, such as DNA-bound water molecules or a subcellular compartment whose elemental composition is closer to water than medium. As D_{wm} depends on the cavity size, the significance the water cavity size in relation biological effects becomes of interest.

The cellular effects of radiation are not completely understood and the definition of radiobiological target has changed over time. Goodhead[60] indicated that microdosimetry theories have presented putative targets on the scale of 1 nm up to several μm. The current evidence points to 3–10 nm (initial DNA damage), 0.1–0.5 μm (subsequent interactions), ≈10 μm (intracellular non-targeted effects) and millimetres or more (inter-cellular bystander effects and influences of the tissue microenvironment)[60]. Detailed track-structure simulations have assumed targets of 10–30 nm, the DNA molecule dimensions and extra space for free radicals released in water, and have correlated a quantity corresponding to linear energy transfer (LET) with RBE[61, 62]. Enger *et al.*[63] assumed μm-sized cell nuclei as the most important quantity with respect to biological effects and Thomson et al.[64] showed that doses to μm-sized targets depend on the composition and geometry of surrounding structures. Oliver and Thomson[65, 66] found that D_{mm} in small volumes (≈10 μm) is dependent on the composition and structure of the surrounding media, potentially rendering D_{wm} clinically meaningless until the effects of tissue composition are better understood.

Beyond the dose-reporting quantities currently employed, and besides their proportional relationship with biological effects, radiotherapy treatments and fundamental radiation knowledge could benefit from a quantity more tightly related to RBE, e.g. cell death probability, biological endpoint or treatment outcome, rather than radiation dose[67, 68]. From radiobiological and physical perspectives, as a number of factors influence the effect of radiation on cell-death (e.g. cell and radiation type, oxygenation, tissue composition, etc) it is important to understand their

underlying relationships to be able to consider their collective impact in a clinical setting. Although in vitro testing can provide some insight, the dynamic biological characteristics of a complex living organism require well designed pre-clinical experiments to separate effects; this topic will be revisited in section 7.2.4.

7.1.5 Proton beam irradiation

In a venture into the light ion irradiation world, **Chapter 6** presented an investigation on the capabilities of a clinical proton system, which features a unique adaptive aperture (AA), concerning the generations of fields small enough for pre-clinical in vivo irradiations. The in silico research was developed through a MC model of the proton beam line nozzle, which consists of an energy modulation system (EMS) and an AA. The EMS enables the 230 MeV beam nominal range to be decreased in multiples of 2.1 mm and the AA allows irradiation fields as small as 5 x 1 mm^2. Irradiation treatment plans were tested with a set of discrete energies, field sizes and beam directions, later compared to photon plans. Although the number of protons which hit the target drops to 1-3%, treatment times below five seconds were found, with good tumour coverage and less damage to the OARs than in photon plans. This study contributed to a deeper understanding of the implications regarding the degradation of the nominal 230 MeV proton beam to low energies, the effect on spot size, dose homogeneity and dose rate.

Proton treatments in Chapter 6 were designed either using low energy fields that stop in the tumour or high energy beams to shoot through. The former allows for a decrease in dose to healthy tissues and might be used to study RBE effects. The latter could be used for small animal proton imaging, for pre-treatment position verification or to improve range uncertainty by directly measuring the animal relative stopping power maps. These two topics will be readdressed in section 7.2.4. The EMS, characterized by a constant range straggling at the Bragg peak, poses a disadvantage for pre-clinical research: it prevents an easy production of sharp beams. Furthermore, it presents an increase in lateral beam spot size for decreasing energies caused by the many plates in front of the beam. Although the AA collimates the beam, there is an intrinsic loss in efficiency when using large spot sizes with small fields: the beam is mostly absorbed by the AA. The intensity is also decreased in the central beam axis, as small angular

deflections in proton trajectories are not negligible for small fields.

Pre-clinical studies are important means to understand the radiobiological properties of ion therapies to effectively realize their potential benefits. Although some aspects, such as the effects of cell survival and proliferation-based RBE values, have been well documented[69], there is a lack of in vivo studies. They could be useful for different radiobiological hypothesis, e.g. RBE dependence on fractionation, differential immune effects with respect to photon beams[70, 71] or, more generally, biological dependence on high LET. Ford et al.[72] have pointed out that irradiation technologies to study these effects are underdeveloped and that there is an urgent need for high-precision image-guided proton radiation delivery systems relevant to animal models. Currently, there are 158 clinical ion beam centres in operation, construction or planning stage[73]. Due to the high cost associated with these facilities, dedicated small animal ion beam systems are unlikely to be developed to a same extent as the photon beam ones. The proper adaptation of clinical facilities for small specimens, including image guidance, fits ideally into this context. However, challenges are expected, such as the acquisition of beam time in the clinical environment.

7.2 Future perspectives

7.2.1 Tissue compositions

As emphasized in section 7.1.1, tissue elemental composition reference data, heavily used on clinical and pre-clinical dose calculations, are based on a few dated studies. Novel estimation techniques could potentially increase accuracy and add information on different populations, gender and age. The non-destructive techniques particle induced x- and gamma-ray emission (PIXE and PIGE) have been suggested to be complementary used to detect heavy element trace quantities and the mass proportions of the lighter ones, respectively. In both approaches, charged particles are accelerated towards a sample of interest: they may cause ionizations and subsequent x-ray emissions, PIXE, or, they may interact with nuclei within the sample and cause gamma-ray emissions, PIGE. Detection of these emissions may reveal the elemental composition of a sample. Additionally, destructive analytical methods include chromatography combined with mass spectrometry, infrared spectroscopy or thermal conductivity detection[13]. Other techniques ex vivo such as neutron activation analysis,

laser-induced breakdown spectroscopy (LIBS), secondary ion mass spectrometry (NanoSIMS), laser ablation-inductively coupled plasma mass spectrometry (LA-ICP-MS) have all been used for elemental composition analysis in different scopes[74, 75].

In vivo techniques can facilitate tissue identification, based on individualized data acquisition instead of reference data. There is a multitude of techniques for composition estimation, divided into levels of increasing complexity: atomic, molecular, cellular, tissue system, and whole body[76]. They range from simple skinfold measurements to bioimpedance analysis, dual energy x-ray absorptiometry, MRI, DECT and in vivo neutron activation analysis (IVNA) methods, such as delayed-γ, prompt-γ and inelastic neutron scattering. In IVNA methods, a subject is placed in a neutron field, its atoms might undergo nuclear reactions and release gamma rays, which are simultaneously measured by scintillation detectors and correlated to elements. Although IVNA measures whole-body compositions, tissue values can be extrapolated through empirical rules. DECT and MRI methods are more convenient and available on an individual basis and yield lower or no radiation dose. The DECT principle is mentioned in Chapter 2. MRI is based on the interaction between hydrogen nuclei (protons) and magnetic fields. Briefly, during a scan, protons absorb energy due to radiofrequency (RF) and release the absorbed energy when RF is ceased: the time it takes for protons to return to their original positions, dependent on interactions with the surrounding medium, can be exploited to yield differences between tissues.

Validation phantoms, human and animal studies for DECT and MRI have been compared to ex vivo data and showed good overall agreement within a distribution[77-82]. These studies support the validity of tissue level estimates and may be considered in vivo reference standards[83]. Yet, there are many sources of uncertainty, such as instrument calibration, stability, subject participation and observer variation. Influence of image quality parameters also play an important role. After the contribution of these factors is weighted, a distribution of values for different tissues and organs is more likely to represent anatomical structures rather than a unique mean value, producing a sound representation of tissue heterogeneity, closer to reality. It would be rather advantageous to adapt MC calculations to spread out or clustered values.

7.2.2 Image quality and dose

Section 7.1.2 showed that a myriad of imaging protocols and algorithms could be characterized to improve image quality and possibly add more value to DECT. However, the benefits would be rather small as current CT imaging technology has inherent limitations, which yield poor intrinsic and soft tissue contrast. Although image quality is sufficient for skeletal topology, the application of contrast agents is typically necessary to visualize differences in soft tissues. This practice has its caveats as it is associated with higher experimental complexity, larger cost and dose calculations effects. To overcome these limitations, relatively new semiconductor x-ray photon counting detectors are expected to bring CT imaging to a new technological generation.

A number of photon counting detectors are commercially available (Medipix and Timepix[84], PILATUS[85], Eiger[86], XPAD[87] and PiXirad[88]) and include a large-area option[89] suitable for small animals[90]. They operate differently from current scintillation-based systems, which detect x-ray photons indirectly through conversion into visible light and integrate the charge from the incoming photons, whereby high energy photons end up with a stronger weight than low energy ones. The semiconductor detectors process incoming photons at the pixel level as single events and weight all photons equally, thus offering higher SNR. They feature adjustable energy thresholds which allow counting incoming photons with dedicated energy for multispectral x-ray imaging. They are practically noiseless and CNR is limited by the number of detected photons. Consequently, soft tissue structures, with low differences in attenuation, can be visualised with high CNR[91]. Figure 7.1 shows images created this technology.

Moving towards this technology has been proven feasible[90] and would allow for the acquisition of improved information of morphological and structural changes of individual organs or tissue structures. It can provide multiple quantitative parameters for distinguishing malignant from benign tumours[92] and improve material analysis through the image-based extraction of tissue compositions, discussed in the previous section. Medipix detectors have been combined with mass spectrometry imaging to demonstrate spatial correlation of molecular and 3D structural information[93]. If used in place of DECT they can provide reduced motion artefacts and radiation doses, and would not require image registration. IR techniques should also be implemented for image reconstruction using

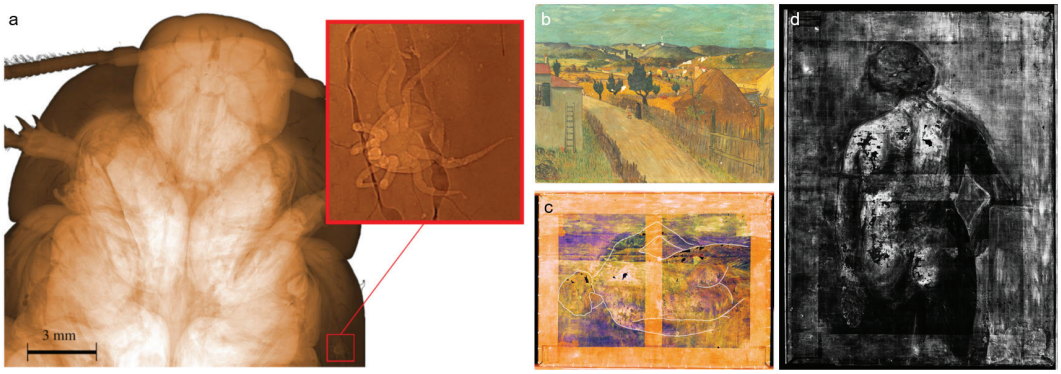

Figure 7.1 – (a) Image of a cockroach taken by the WidePIX detector. The zoom detail shows veins and a tick parasite in the inset. Reproduced with kind permission from Jakubek et al. 2014[89]. (b-d) The use of these detectors in artworks. (b) The painting of La Crau with a View of Montmajour, with the signature Vincent, was subject to material-sensitive X-ray radiography. (c) the figure of a female nude from behind was found underneath the painting, similar to other van Gogh works. (d) The X-ray images are able to show the distribution of individual pigments across the image and the way they were applied. Using energy channel separation to achieve individual layers and materials the materials that are only related to a target layer of paint become evident. This method allows a completely new way of working with X-ray radiography using advanced pixel detectors.

this technology. Currently, the lack of a commercial system developed with hardware and software for these detectors, limit their scope to fundamental research and a few commercial applications.

In addition to hardware, image reconstruction techniques are likely to undergo substantial developments. In Chapter 3, a software platform for image reconstruction was presented. Briefly, the software received CBCT projections, encoded as an intermediate representation of the object in the detector domain, and reconstructed them into an image by the invertion of the encoding function. Analytically, it gradually solved the Radon inversion, and iteratively it used a cost function, which considered prior knowledge of projections or the image and noise properties. Image reconstruction is a challenging process: projections are acquired by imperfect and noisy detectors; iterative techniques have simplistic noise models and involve time-consuming steps. Artificial intelligence (AI) methods have been used for the entire image reconstruction process or to act on specific artefact and noise corrections.

Data-driven supervised learning frameworks have recently been proposed for image reconstruction. The automated transform by manifold approximation, AUTOMAP[94], learns a mapping between the detector and

the image domain, derived from training data. It is implemented with a deep neural network, which learns different reconstruction transforms for various imaging acquisition strategies, using similar network architecture and parameters. It generates images with reduced noise and artefacts when compared with conventional methods. As AUTOMAP does not handle large reconstruction matrices, the Radon inversion approximation, RAINAP[95], was proposed by a different group. It represents a unified framework for Radon inversion using neural networks. The algorithm first applies filtering and back-projection operations with two learnable appropriative network layers to perform the domain transform. Subsequently, it uses a convolutional neural network to refine the reconstruction performance. Besides algorithms targeting the reconstruction problem, several deep learning methods, including neural networks have been proposed to act on image quality parameters. For example, deep learning techniques have been used to minimize the mean-squared error between an artificially denoised CT image and the ground truth under generic penalties[96]; denoising based on the generative adversarial networks, which focus on migrating the noise distribution from statistically strong to weak, have also been proposed[97] and convolutional neural network (CNN) or deep neural networks for sparse-view artefact reduction.

AI applied to medical imaging has been exponentially expanding and is likely to change several aspects of this field[98, 99]: it is a suitable candidate for solving ill-posed inverse problems, and, as CT scans are routinely collected, large data sets are readily available. Current commercial software does not treat image artefacts with machine learning (ML) techniques, although it is expected to happen in the near future, ML requires massive computational resources, including state-of-the-art GPUs for data training with adequate and representative data. Pre-clinically, it is expected to yield advantageous results as small animals share more similarities than humans. A proper image database is necessary and still represents a drawback as most research institutions lack an organized database. Machine learning techniques have also been proposed for noise reduction in low-dose CT, therefore reducing the subject imaging dose.

Imaging dose is a concern and a potential limiting factor if successive CT scans would influence experimental outcome. Pre-clinical irradiators have recently been adapted to support bioluminescence imaging (BLI) integrated in the same frame of reference of the CT scanner. BLI is a type of molecular imaging, where a sensitive optical camera in a light-tight

environment records weak light sources originating up to a few centimetres deep in tissues[100]. It has a high signal-to-noise ratio, fast acquisition times, it is easy to use and cost-effective. Optical imaging has become increasingly attractive due to the availability of targeted probes, probes activated due to enzymatic reactions or probes that can be produced by cells themselves in the form of bioluminescent enzymes[101]. It does not present additional radiation burden to the animals and can be used to evaluate longitudinal tumour growth and to estimate tumour size. However, due to low spatial resolution, typically 1-2 mm, it is not suited for morphological and somewhat suited for functional imaging[102]. It generates a two-dimensional (2D) planar image. Recent efforts have been put on 3D image reconstruction of this technique, which is also expected to benefit from AI techniques[103].

7.2.3 From target margins to treatment adaptation

The research on target margins could spawn a couple of prospective studies. Firstly, the recipe described in Chapter 2 used DVH metrics to yield radiotherapy treatment margins. A thorough investigation on the radiosensitivity of different murine OARs based on current irradiation technology, considering dose rates and dynamic treatments could promote margin recommendations for different sites. And secondly, the effect of respiratory motion on the CT image blurring could be fully investigated through projection based 4D-CBCT simulation, using the MC code GATE, as it provides good capabilities for imaging simulation.

Another topic mentioned at the end of the discussion regarding Chapter 4 was adaptive radiotherapy. A verification system to quantify possible discrepancies between planned and delivered dose could bring extensive benefits to this field. Discrepancies with respect to planned dose can occur due to motion between imaging and treatment and due to anatomical changes in the course of treatment. The clinical practice with photon beams has adapted the imaging panel, also called electronic portal imaging device (EPID), to be a verification tool for different scenarios: before, during or after treatment and with or without the subject present during the verifications. There are four main scenarios [104] presented in Figure 7.2.

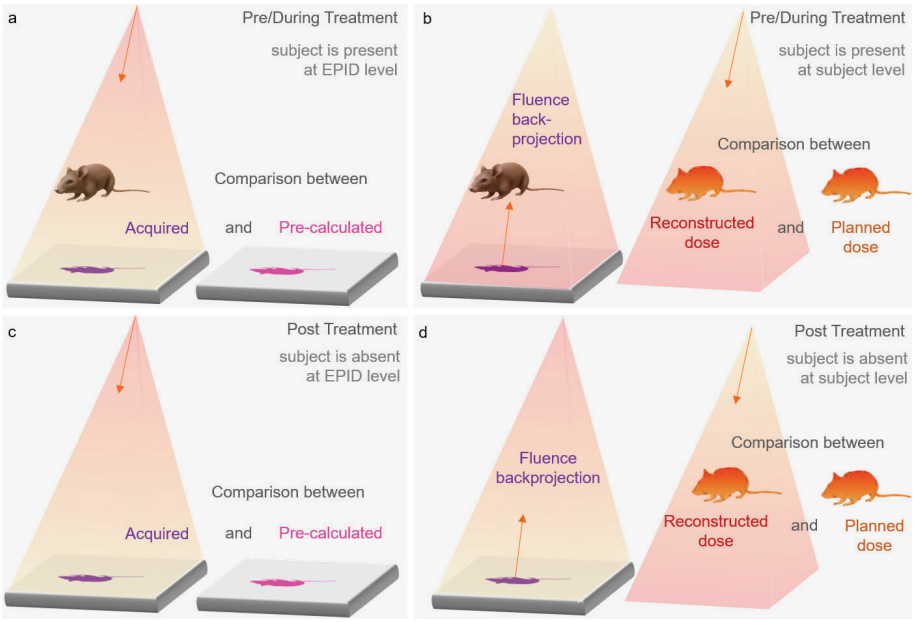

Figure 7.2 – Verification scenarios: (a) detector level with subject: an image is acquired and compared to a pre-calculated one, based on the treatment plan; (b) at subject level with subject: the photon fluence is measured at detector level after its passage through the subject and is back-projected upwards through the subject; an independent dose calculation is performed and the 3D reconstructed dose distribution is compared to the planned dose; (c) at detector level without subject: an image is acquired and compared to a pre-calculated one, errors related to the subject cannot be detected but it can be verified if the planned image corresponds to the delivered one and (d) at subject level without subject: fluence is back-projected without the subject and photons are subsequently forward propagated for a dose calculation in the CT image, which is compared to the planned dose.

Treatment verification implementation requires a framework for image prediction and comparison, fluence back-projection, dose reconstruction and the conversion of image into dose. Furthermore, a number of measurements and calibrations are necessary to act on possible sources of errors inherent to the image detector, such as warm-up time, radiation dose history effect, stability and short- and long-term reproducibility, gantry angle dependency, output factor and response linearity. Other sources of dose delivery errors rely on operator- and system-related factors that can individually or cumulatively contribute to dosimetric errors, such as incorrect filter selection, gantry sag and wobble, couch rotation, and collimator misalignment. Pre-clinically, dose delivery has been investigated

using dosimeters, such as oxide semiconductor field effect transistors (MOSFETs) surgically implanted in mice or Gafchromic film for narrow kV beams[105, 106]. Regarding the use of EPIDSs, Granton et al.[107] investigated the accuracy of the treatment plan delivery using a MC model to simulate the flat panel image. Simulation was compared to measurements to verify that intended treatment dose agreed with the delivered treatment dose. Dose delivery errors resulting from intrafraction motion were also assessed. Anvari et al.[108, 109] quantified the dosimetric characterization of the EPID at kV x-ray energies in a year-long period and, in a subsequent study, they converted EPID images into 2D dose maps at the detector plane and used these maps to calculate 2D dose distribution at the exit surface in phantoms. Accuracy of transit and exit dose distributions were independently validated with ion chamber and film measurements. Further development of these techniques, including 3D or 4D models could increase treatment conformity and add more value to the comparison with or the translation to clinical practice.

7.2.4 Dose reporting

Previously mentioned on section 7.1.5, the debate over which dose reporting quantity to favour in radiotherapy D_{mm} or D_{wm} lacks quantitative radiobiological data. This information could potentially establish which one best correlates with biological damage. Precise radiotherapy experiments on complex living systems have only recently become feasible through novel pre-clinical irradiation platforms. Considering the opportunity to investigate a fundamental scientific question on highly controlled experimental conditions, the most immediate future work following the discoveries of this thesis should be to investigate the influence of the physical aspects on cell death caused by radiation dose, particularly the impact of dose prescribed using different quantities. A study protocol has been designed along with the radiobiology department. The aim is to analyse acute radiation effects from doses prescribed with D_{mm} and D_{wm}. Several essays are foreseen, e.g. clonogenic survival, gut toxicity, blood profile and bone marrow leucocytes and lymphocytes. A range of kV energies should be applied, as RBE is expected to increase for lower energies, yet not excessively low as dose-rate effects should not interfere. Greater radiation damage difference is expected for lower energies. Gaining insight in this will provide essential data towards a fundamental understanding of how living tissue interacts with radiation.

7.2.5 Light ions

Similar to photon platforms, clinically relevant pre-clinical proton research requires image guidance. Chapter 6 and section 7.1.5 showed the feasibility of a clinical set-up used pre-clinically and concluded that high energy beams can be used to shoot through the specimens and enable proton imaging or range verification. Proton imaging typically offers limited spatial resolution due to Coulomb scattering: on their way through matter, protons are slowed down in interactions with atomic electrons and deflected from their initial direction in electromagnetic interactions with atomic nuclei, resulting in an angular spread from many deflections. Sophisticated methods, such as single particle tracking or magnetic optics can improve image resolution[110]. Muller et al. suggested a method for dual-energy proton radiography using enhancement of residual energy distribution for different proton energies. The images show structures dominated by energy absorption or scattering of protons in the object. Although their images lack spatial resolution, they are sufficient for position verification, provide low imaging dose, use same frame of reference of the treatment beam and the absorption images allow range verification within the animal. This technique can be further exploited into proton-CT imaging.

Chapter 6 also concluded that lower energy proton treatments, designed to stop at the tumour could be used to study RBE effects. In comparison to photons, light ion beams produce increased energy deposition with penetration depth and intensify biological effectiveness with enhanced ionization density in individual particle tracks, where DNA damage becomes clustered and more difficult to repair. Radiobiological and biophysical studies have improved the RBE understanding of light ions and dose-localizing properties. However, in a recent review, Paganetti[111] has challenged the whole concept of the proton RBE value of 1.1. He considered it "generic, spatially invariant within tumours and normal tissues [which] disregards the evidence that proton RBE varies with LET, physiological and biological factors, and clinical endpoint". He further analysed the relationship between RBE and dose, biological endpoint and physical properties of proton beams and concluded that there are considerable uncertainties in RBE values, where additional radiobiological data is necessary to reduce uncertainties to clinically acceptable levels. Besides uncertainties in RBE, proton treatments could benefit from advanced research on fractionation schemes, radioresistance and adjuvant therapies[112].

In parallel, there has been a crescent development of targeted radiopharmaceutical therapies using alpha, beta, Auger and positron emitters, due to a higher availability of isotope production. Here, instead of an external hadron beam, a pharmaceutical labelled with a radioisotope binds to specific target cells and may allow fatal dose delivery to malignant structures while sparing the majority of healthy tissue. For clinical feasibility, a radionuclide must have a suitable emission at a reasonable branching ratio, suitable chemical properties to allow attachment to relevant ligands and an appropriate half-life. This field largely relies on pre-clinical research as a pipeline for phase I clinical trials and the dosimetry is heavily based on imaging, using functional techniques such as SPECT/CT, PET/CT and autoradiography. Especially for rare radionuclides, which show promising results in animal models, such as Actinum-225[113, 114] and Astatine-211[115], it should be advantageous to research the correlation of these new techniques with standard external beam irradiation regarding treatment outcome. Moreover, research on targeted radionuclide therapy as adjuvant technique can also be beneficial.

7.3 Final remarks

Regardless of the immense possibilities pre-clinical radiotherapy offers, it is unavoidable to acknowledge that small animals are not humans. Frequently, their unique characteristics favour research, e.g. ability to manipulate their phenotype and genotype. However, the vast majority of studies are not replicated in humans[116]. In a recent review, Koontz et al.[117] pointed to some issues in successful pre-clinical translation to standard treatments, summarized in **Table 7.1.** Besides the difficulties in matching human and mice biology, radiation delivery and physical properties of the irradiators are often different from the clinic. Considering strategies to increase pre-clinical research productivity, they encouraged the use of orthotopic models, biomarkers, pharmacodynamic read-outs, robust imaging and computational modelling. They concluded that the selection of mice should favour "a direct bilateral link (...) to the molecular characteristics of the human condition and that of the appropriate mouse strain" and pre-clinical and clinical research should work as a cycle "considering the biology which needs to be represented in the model, tailoring the physics of the irradiation as close to the human situation as possible and acknowledging the limitations that cannot be overcome".

Finally, for successful pre-clinical research from physical and biological standpoints, the multidisciplinarity of this field cannot be forsaken. Progress can only be achieved through the combined efforts and wisdom inherent of different fields.

CONCERNS	EXPLANATION
	biological
Treatment naıve animals	Mutational stress caused by heavily pre-treated human cancer
Immune status	Immune system part of radiation response
Inherent biology differences	Molecular biology differences between mouse and human
	physical
Field Size	Dose accuracy similarity to human anatomical borders
Radiation dose/ fractionation/dose rate	Radiobiology differences
Irradiator energy differences	kV planning software for accurate dose prediction
Animal setup	OAR Anesthesia: air mix
Radiation QA procedures	Frequency of testing

Table 7.1 – Considerations with small animal radiotherapy models. Reproduced with kind permission from Koontz *et al.*[117]

7.4 References

[1] F. Verhaegen, L. Dubois, S. Gianolini, M.A. Hill, C.P. Karger, K. Lauber, K.M. Prise, D. Sarrut, D. Thorwarth, C. Vanhove, B. Vojnovic, R. Weersink, J.J. Wilkens, D. Georg, ESTRO ACROP: Technology for precision small animal radiotherapy research: Optimal use and challenges, Radiother Oncol, 126 (2018) 471-478.

[2] B.R. Walters, R. Kramer, I. Kawrakow, Dose to medium versus dose to water as an estimator of dose to sensitive skeletal tissue, Phys Med Biol, 55 (2010) 4535-4546.

[3] F. Verhaegen, P. Granton, E. Tryggestad, Small animal radiotherapy research platforms, Phys Med Biol, 56 (2011) R55-83.

[4] J. Bäurle, J. Kučera, S. Frischmuth, M. Lambertz, K. Kranda, Dynamics of Trace Element Concentration During Development and Excitotoxic Cell Death in the Cerebellum of Lurcher Mutant Mice, Brain Pathology, 19 (2009) 586-595.

[5] M. Anniko, R. Wroblewski, Elemental Composition of the Developing Inner Ear, Annals of Otology, Rhinology & Laryngology, 90 (1981) 25-32.

[6] N. Debernardi, R.B. Roijers, R. Krams, R. De Crom, P.H.A. Mutsaers, G.J. Van Der Vusse, Microcalcifications in atherosclerotic lesion of apolipoprotein E-deficient mouse, International Journal of Experimental Pathology, 91 (2010) 485-494.

[7] J.M. Moran, D.W. Nigg, F.J. Wheeler, W.F. Bauer, Macroscopic geometric heterogeneity effects in radiation dose distribution analysis for boron neutron capture therapy, Medical Physics, 19 (1992) 723-732.

[8] M. Długaszek, K. Kopczyński, Elemental Composition of Muscle Tissue of Wild Animals from Central Region of Poland, International Journal of Environmental Research, 7 (2013) 973-978.

[9] K. Buddhachat, S. Klinhom, P. Siengdee, J.L. Brown, R. Nomsiri, P. Kaewmong, C. Thitaram, P. Mahakkanukrauh, K. Nganvongpanit, Elemental Analysis of Bone, Teeth, Horn and Antler in Different Animal Species Using Non-Invasive Handheld X-Ray Fluorescence, PLoS One, 11 (2016) e0155458.

[10] ICRP, Report of the Task Group on Reference Man, Pergamon Press, Oxford., ICRP Publication 23 (1975).

[11] D.R. White, J. Booz, R.V. Griffith, J.J. Spokas, I.J. Wilson, Report 44, Journal of the International Commission on Radiation Units and Measurements, os23 (1989) NP-NP.

[12] H.Q. Woodard, D.R. White, Bone models for use in radiotherapy dosimetry, Br J Radiol, 55 (1982) 277-282.

[13] D. Mann-Krzisnik, F. Verhaegen, S.A. Enger, The influence of tissue composition uncertainty on dose distributions in brachytherapy, Radiother Oncol, 126 (2018) 394-410.

[14] L.E. Schyns, D.B. Eekers, B. van der Heyden, I.P. Almeida, A. Vaniqui, F. Verhaegen, Murine vs human tissue compositions: implications of using human tissue compositions for photon energy absorption in mice, Br J Radiol, DOI 10.1259/bjr.20180454(2018) 20180454.

[15] J.M. Boone, O. Velazquez, S.R. Cherry, Small-animal X-ray dose from micro-CT, Mol Imaging, 3 (2004) 149-158.

[16] S.K. Carlson, K.L. Classic, C.E. Bender, S.J. Russell, Small animal absorbed radiation dose from serial micro-computed tomography imaging, Mol Imaging Biol, 9 (2007) 78-82.

[17] C.D. Johnstone, M. Bazalova-Carter, MicroCT imaging dose to mouse organs using a validated Monte Carlo model of the small animal radiation research platform (SARRP), Phys Med Biol, 63 (2018) 115012.

[18] L.Y. Du, J. Umoh, H.N. Nikolov, S.I. Pollmann, T.Y. Lee, D.W. Holdsworth, A quality assurance phantom for the performance evaluation of volumetric micro-CT systems, Phys Med Biol, 52 (2007) 7087-7108.

[19] C.D. Johnstone, P. Lindsay, E.E. Graves, E. Wong, J.R. Perez, Y. Poirier, Y. Ben-Bouchta, T. Kanesalingam, H. Chen, A.E. Rubinstein, K. Sheng, M. Bazalova-Carter, Multi-institutional MicroCT image comparison of image-guided small animal irradiators, Phys Med Biol, 62 (2017) 5760-5776.

[20] C.M. Ma, C.W. Coffey, L.A. DeWerd, C. Liu, R. Nath, S.M. Seltzer, J.P. Seuntjens, M. American Association of Physicists in, AAPM protocol for 40-300 kV x-ray beam dosimetry in radiotherapy and radiobiology, Med Phys, 28 (2001) 868-893.

[21] S.C.C. Klevenhagen, R.J. Aukett, R.M. Harrison, C. Moretti, A.E. Nahum, K.E. Rosser, The IPEMB code of practice for the determination of absorbed dose for x-rays below 300 kV generating potential (0.035 mm Al - 4 mm Cu HVL; 10 - 300 kV generating potential), Physics in Medicine and Biology, 41 (1996) 2605-2625.

[22] R.J. Aukett, J.E. Burns, A.G. Greener, R.M. Harrison, C. Moretti, A.E. Nahum, K.E. Rosser, I.W. Party, Addendum to the IPEMB code of practice for the determination of absorbed dose for x-rays below 300 kV generating potential (0.035 mm Al-4 mm Cu HVL), Phys Med Biol, 50 (2005) 2739-2748.

[23] IAEA, Implementation of the International Code of Practice on Dosimetry in Radiotherapy (TRS 398): Review of Test Results, INTERNATIONAL ATOMIC ENERGY AGENCY, Vienna, 2005.

[24] S.H. Bartling, J. Kuntz, W. Semmler, Gating in small-animal cardio-thoracic CT, Methods, 50 (2010) 42-49.

[25] M.A. Hill, B. Vojnovic, Implications of respiratory motion for small animal image-guided radiotherapy, Br J Radiol, 90 (2017) 20160482.

[26] C.T. Badea, B. Fubara, L.W. Hedlund, G.A. Johnson, 4-D Micro-CT of the Mouse Heart, Molecular Imaging, 4 (2005).

[27] G. Cao, L.M. Burk, Y.Z. Lee, X. Calderon-Colon, S. Sultana, J. Lu, O. Zhou, Prospective-gated cardiac micro-CT imaging of free-breathing mice using carbon nanotube field emission x-ray, Med Phys, 37 (2010) 5306-5312.

[28] I.G. Buliev, C.T. Badea, Z. Kolitsi, N. Pallikarakis, Estimation of the heart respiratory motion with applications for cone beam computed tomography imaging: a simulation study, IEEE Transactions on Information Technology in Biomedicine, 7 (2003) 404-411.

[29] E.B. Walters, K. Panda, J.A. Bankson, E. Brown, D.D. Cody, Improved method ofin vivorespiratory-gated micro-CT imaging, Physics in Medicine and Biology, 49 (2004) 4163-4172.

[30] C. Badea, L.W. Hedlund, G.A. Johnson, Micro-CT with respiratory and cardiac gating, Med Phys, 31 (2004) 3324-3329.

[31] D. Cavanaugh, E. Johnson, R.E. Price, J. Kurie, E.L. Travis, D.D. Cody, In Vivo Respiratory-Gated Micro-CT Imaging in Small-Animal Oncology Models, Molecular Imaging, 3 (2004).

[32] N.L. Ford, H.N. Nikolov, C.J. Norley, M.M. Thornton, P.J. Foster, M. Drangova, D.W. Holdsworth, Prospective respiratory-gated micro-CT of free breathing rodents, Med Phys, 32 (2005) 2888-2898.

[33] L.M. Burk, Y.Z. Lee, J.M. Wait, J. Lu, O.Z. Zhou, Non-contact respiration monitoring for in-vivo murine micro computed tomography: characterization and imaging applications, Phys Med Biol, 57 (2012) 5749-5763.

[34] M. Drangova, N.L. Ford, S.A. Detombe, A.R. Wheatley, D.W. Holdsworth, Fast retrospectively gated quantitative four-dimensional (4D) cardiac micro computed tomography imaging of free-breathing mice, Invest Radiol, 42 (2007) 85-94.

[35] S.H. Bartling, W. Stiller, M. Grasruck, B. Schmidt, P. Peschke, W. Semmler, F. Kiessling, Retrospective motion gating in small animal CT of mice and rats, Invest Radiol, 42 (2007) 704-714.

[36] N.L. Ford, A.R. Wheatley, D.W. Holdsworth, M. Drangova, Optimization of a retrospective technique for respiratory-gated high speed micro-CT of free-breathing rodents, Phys Med Biol, 52 (2007) 5749-5769.

[37] D. Ertel, Y. Kyriakou, R.M. Lapp, W.A. Kalender, Respiratory phase-correlated micro-CT imaging of free-breathing rodents, Phys Med Biol, 54 (2009) 3837-3846.

[38] T.H. Farncombe, Software-based respiratory gating for small animal conebeam CT, Med Phys, 35 (2008) 1785-1792.

[39] J. Hu, S.T. Haworth, R.C. Molthen, C.A. Dawson, Dynamic small animal lung imaging via a postacquisition respiratory gating technique using micro-cone beam computed tomography, Acad Radiol, 11 (2004) 961-970.

[40] M.A. Hill, J.M. Thompson, A. Kavanagh, I.D.C. Tullis, R.G. Newman, J. Prentice, J. Beech, S. Gilchrist, S. Smart, E. Fokas, B. Vojnovic, The Development of Technology for Effective Respiratory-Gated Irradiation Using an Image-Guided Small Animal Irradiator, Radiat Res, 188 (2017) 247-263.

[41] A.M. Frelin-Labalme, V. Beaudouin, Development of a dynamic phantom and investigation of mobile target imaging and irradiation in preclinical small animal research, Br J Radiol, 90 (2017) 20160442.

[42] A.M. Frelin, V. Beaudouin, C. Le Deroff, T. Roger, Implementation and evaluation of respiratory gating in small animal radiotherapy, Phys Med Biol, 63 (2018) 215024.

[43] T.E. Burlin, F.K. Chan, The effect of the wall on the Fricke dosemeter, The International Journal of Applied Radiation and Isotopes, 20 (1969) 767-775.

[44] A. Janssens, G. Eggermont, R. Jacobs, G. Thielens, Spectrum perturbation and energy deposition models for stopping power ratio calculations in general cavity theory, Physics in Medicine and Biology, 19 (1974) 619-630.

[45] L.H. Gray, The Absorption of Penetrating Radiation, Proceedings of the Royal Society A: Mathematical, Physical and Engineering Sciences, 122 (1929) 647-668.

[46] L.H. Gray, E. Rutherford, An ionization method for the absolute measurement of γ-ray energy, Proceedings of the Royal Society of London. Series A - Mathematical and Physical Sciences, 156 (1936) 578-596.

[47] L.V. Spencer, F.H. Attix, A Theory of Cavity Ionization, Radiation Research, 3 (1955).

[48] P.R.J. Burch, Cavity Ion Chamber Theory, Radiation Research, 3 (1955).

[49] P.R.J. Burch, Comment on Recent Cavity Ionization Theories, Radiation Research, 6 (1957).

[50] A.E. Nahum, Water/air mass stopping power ratios for megavoltage photon and electron beams, Physics in Medicine and Biology, 23 (1978) 24-38.

[51] P.R. Almond, P.J. Biggs, B.M. Coursey, W.F. Hanson, M.S. Huq, R. Nath, D.W. Rogers, AAPM's TG-51 protocol for clinical reference dosimetry of high-energy photon and electron beams, Med Phys, 26 (1999) 1847-1870.

[52] H. Bouchard, J. Seuntjens, Chapter 4: Applications of Monte Carlo to Radiation Dosimetry, CRC Press, Boca Raton, FL, 2013.

[53] T.E. Burlin, A general theory of cavity ionisation, Br J Radiol, 39 (1966) 727-734.

[54] A. Janssens, The fundamental constraint of cavity theory, Physics in Medicine and Biology, 29 (1984) 1157-1158.

[55] A.F. Bielajew, D.W.O. Rogers, A.E. Nahum, The Monte Carlo simulation of ion chamber response to60Co-resolution of anomalies associated with interfaces, Physics in Medicine and Biology, 30 (1985) 419-427.

[56] L. Zheng-Ming, An Electron Transport Theory of Cavity Ionization, Radiation Research, 84 (1980).

[57] R. Jacques, J. Wong, R. Taylor, T. McNutt, Real-time dose computation: GPU-accelerated source modeling and superposition/convolution, Med Phys, 38 (2011) 294-305.

[58] N. Cho, P. Tsiamas, E. Velarde, E. Tryggestad, R. Jacques, R. Berbeco, T. McNutt, P. Kazanzides, J. Wong, Validation of GPU-accelerated superposition-convolution dose computations for the Small Animal Radiation Research Platform, Med Phys, 45 (2018) 2252-2265.

[59] N.B. Cho, J. Wong, P. Kazanzides, Fast Inverse Planning of Beam Directions and Weights for Small Animal Radiotherapy, IEEE Transactions on Radiation and Plasma Medical Sciences, 2 (2018) 215-222.

[60] D.T. Goodhead, Energy deposition stochastics and track structure: what about the target?, Radiat Prot Dosimetry, 122 (2006) 3-15.

[61] D.T. Goodhead, Initial Events in the Cellular Effects of Ionizing Radiations: Clustered Damage in DNA, International Journal of Radiation Biology, 65 (1994) 7-17.

[62] L. Lindborg, M. Hultqvist, A. Carlsson Tedgren, H. Nikjoo, Lineal energy and radiation quality in radiation therapy: model calculations and comparison with experiment, Phys Med Biol, 58 (2013) 3089-3105.

[63] S.A. Enger, A. Ahnesjo, F. Verhaegen, L. Beaulieu, Dose to tissue medium or water cavities as surrogate for the dose to cell nuclei at brachytherapy photon energies, Phys Med Biol, 57 (2012) 4489-4500.

[64] R.M. Thomson, A.C. Tedgren, J.F. Williamson, On the biological basis for competing macroscopic dose descriptors for kilovoltage dosimetry: cellular dosimetry for brachytherapy and diagnostic radiology, Phys Med Biol, 58 (2013) 1123-1150.

[65] P.A. Oliver, R.M. Thomson, A Monte Carlo study of macroscopic and microscopic dose descriptors for kilovoltage cellular dosimetry, Phys Med Biol, 62 (2017) 1417-1436.

[66] P.A.K. Oliver, R.M. Thomson, Cavity theory applications for kilovoltage cellular dosimetry, Phys Med Biol, 62 (2017) 4440-4459.

[67] M. Podesta, Time dependent verification of dynamic external beam radiotherapy, School for Oncology and Developmental Biology, Radiotherapy Research, Maastricht University, Maastricht, 2016, pp. 170.

[68] M.M. Ahmed, C.N. Coleman, M. Mendonca, S. Bentzen, B. Vikram, S.M. Seltzer, D. Goodhead, C. Obcemea, R. Mohan, K.M. Prise, J. Capala, D. Citrin, G. Kao, M. Aryankalayil, I. Eke, J.C. Buchsbaum, P.G.S. Prasanna, F.F. Liu, Q.T. Le, B. Teicher, D.G. Kirsch, D. Smart, J. Tepper, S. Formenti, D. Haas-Kogan, D. Raben, J. Mitchell, Workshop Report for Cancer Research: Defining the Shades of Gy: Utilizing the Biological Consequences of Radiotherapy in the Development of New Treatment Approaches-Meeting Viewpoint, Cancer Res, 78 (2018) 2166-2170.

[69] H. Paganetti, A. Niemierko, M. Ancukiewicz, L.E. Gerweck, M. Goitein, J.S. Loeffler, H.D. Suit, Relative biological effectiveness (RBE) values for proton beam therapy, International Journal of Radiation Oncology*Biology*Physics, 53 (2002) 407-421.

[70] B. Jones, R.G. Dale, Estimation of optimum dose per fraction for high LET radiations: Implications for proton radiotherapy, International Journal of Radiation Oncology*Biology*Physics, 48 (2000) 1549-1557.

[71] S. Girdhani, R. Sachs, L. Hlatky, Biological effects of proton radiation: what we know and don't know, Radiat Res, 179 (2013) 257-272.

[72] E. Ford, R. Emery, D. Huff, M. Narayanan, J. Schwartz, N. Cao, J. Meyer, R. Rengan, J. Zeng, G. Sandison, G. Laramore, N. Mayr, An image-guided precision proton radiation platform for preclinical in vivo research, Phys Med Biol, 62 (2017) 43-58.

[73] PTCOG, Particle therapy facilities in clinical operation (last update: February 2019), 2018.

[74] B. Busser, S. Moncayo, J.-L. Coll, L. Sancey, V. Motto-Ros, Elemental imaging using laser-induced breakdown spectroscopy: A new and promising approach for biological and medical applications, Coordination Chemistry Reviews, 358 (2018) 70-79.

[75] J. Nunez, R. Renslow, J.B. Cliff, 3rd, C.R. Anderton, NanoSIMS for biological applications: Current practices and analyses, Biointerphases, 13 (2017) 03B301.

[76] M.O. Fosbol, B. Zerahn, Contemporary methods of body composition measurement, Clin Physiol Funct Imaging, 35 (2015) 81-97.

[77] N. Abate, D. Burns, R.M. Peshock, A. Garg, S.M. Grundy, Estimation of adipose tissue mass by magnetic resonance imaging: validation against dissection in human cadavers, Journal of Lipid Research, 35 (1994) 1490-1496.

[78] A. Aliprantis, J. Wang, R.N. Baumgartner, R.N. Pierson, Jr, S. Lichtman, S.B. Heymsfield, Y. Kamen, Body composition of humans: comparison of two improved four-compartment models that differ in expense, technical complexity, and radiation exposure, The American Journal of Clinical Nutrition, 52 (1990) 52-58.

[79] E.W. Demerath, W. Shen, M. Lee, A.C. Choh, S.A. Czerwinski, R.M. Siervogel, B. Towne, Approximation of total visceral adipose tissue with a single magnetic resonance image, Am J Clin Nutr, 85 (2007) 362-368.

[80] M. Patino, A. Prochowski, M.D. Agrawal, F.J. Simeone, R. Gupta, P.F. Hahn, D.V. Sahani, Material Separation Using Dual-Energy CT: Current and Emerging Applications, Radiographics, 36 (2016) 1087-1105.

[81] G. Landry, K. Parodi, J.E. Wildberger, F. Verhaegen, Deriving concentrations of oxygen and carbon in human tissues using single- and dual-energy CT for ion therapy applications, Phys Med Biol, 58 (2013) 5029-5048.

[82] G. Landry, P.V. Granton, B. Reniers, M.C. Ollers, L. Beaulieu, J.E. Wildberger, F. Verhaegen, Simulation study on potential accuracy gains from dual energy CT tissue segmentation for low-energy brachytherapy Monte Carlo dose calculations, Phys Med Biol, 56 (2011) 6257-6278.

[83] S.B. Heymsfield, Z. Wang, R.N. Baumgartner, R. Ross, Human body composition: advances in models and methods, Annu Rev Nutr, 17 (1997) 527-558.

[84] X. Llopart, R. Ballabriga, M. Campbell, L. Tlustos, W. Wong, Timepix, a 65k programmable pixel readout chip for arrival time, energy and/or photon counting measurements, Nuclear Instruments and Methods in Physics Research Section A: Accelerators, Spectrometers, Detectors and Associated Equipment, 581 (2007) 485-494.

[85] B. Henrich, A. Bergamaschi, C. Broennimann, R. Dinapoli, E.F. Eikenberry, I. Johnson, M. Kobas, P. Kraft, A. Mozzanica, B. Schmitt, PILATUS: A single photon counting pixel detector for X-ray applications, Nuclear Instruments and Methods in Physics Research Section A: Accelerators, Spectrometers, Detectors and Associated Equipment, 607 (2009) 247-249.

[86] R. Dinapoli, A. Bergamaschi, B. Henrich, R. Horisberger, I. Johnson, A. Mozzanica, E. Schmid, B. Schmitt, A. Schreiber, X. Shi, G. Theidel, EIGER: Next generation single photon counting detector for X-ray applications, Nuclear Instruments and Methods in Physics Research Section A: Accelerators, Spectrometers, Detectors and Associated Equipment, 650 (2011) 79-83.

[87] J.F. Berar, N. Boudet, P. Breugnon, B. Caillot, B. Chantepie, J.C. Clemens, P. Delpierre, B. Dinkespiller, S. Godiot, C. Meessen, M. Menouni, C. Morel, P. Pangaud, E. Vigeolas, S. Hustache, K. Medjoubi, XPAD3 hybrid pixel detector applications, Nuclear Instruments and Methods in Physics Research Section A: Accelerators, Spectrometers, Detectors and Associated Equipment, 607 (2009) 233-235.

[88] R. Bellazzini, G. Spandre, A. Brez, M. Minuti, M. Pinchera, P. Mozzo, Chromatic X-ray imaging with a fine pitch CdTe sensor coupled to a large area photon counting pixel ASIC, Journal of Instrumentation, 8 (2013) C02028-C02028.

[89] J. Jakubek, M. Jakubek, M. Platkevic, P. Soukup, D. Turecek, V. Sykora, D. Vavrik, Large area pixel detector WIDEPIX with full area sensitivity composed of 100 Timepix assemblies with edgeless sensors, Journal of Instrumentation, 9 (2014) C04018-C04018.

[90] J. Dudak, J. Zemlicka, F. Krejci, S. Polansky, J. Jakubek, J. Mrzilkova, M. Patzelt, J. Trnka, X-ray micro-CT scanner for small animal imaging based on Timepix detector technology, Nuclear Instruments and Methods in Physics Research Section A: Accelerators, Spectrometers, Detectors and Associated Equipment, 773 (2015) 81-86.

[91] J. Dudak, J. Zemlicka, J. Karch, M. Patzelt, J. Mrzilkova, P. Zach, Z. Hermanova, J. Kvacek, F. Krejci, High-contrast X-ray micro-radiography and micro-CT of ex-vivo soft tissue murine organs utilizing ethanol fixation and large area photon-counting detector, Sci Rep, 6 (2016) 30385.

[92] M.-L. Chen, X.-T. Li, Y.-Y. Wei, L.-P. Qi, Y.-S. Sun, Can spectral computed tomography imaging improve the differentiation between malignant and benign pulmonary lesions manifesting as solitary pure ground glass, mixed ground glass, and solid nodules?, Thoracic Cancer, 10 (2019) 234-242.

[93] E.S. E Schioppa Jr, Jr., S. Ellis, A.L. Bruinen, J. Visser, R.M.A. Heeren, J. Uher, E. Koffeman, Combined X-ray CT and mass spectrometry for biomedical imaging applications, Journal of Instrumentation, 9 (2014) C04029-C04029.

[94] B. Zhu, J.Z. Liu, S.F. Cauley, B.R. Rosen, M.S. Rosen, Image reconstruction by domain-transform manifold learning, Nature, 555 (2018) 487-492.

[95] J. He, J. Ma, Radon Inversion via Deep Learning, arXiv e-prints, 2018.

[96] Y. Ge, Q. Zhang, Z. Hu, J. Chen, W. Shi, H. Zheng, D. Liang, Deconvolution-Based Backproject-Filter (BPF) Computed Tomography Image Reconstruction Method Using Deep Learning Technique, arXiv e-prints, 2018.

[97] Q. Yang, P. Yan, Y. Zhang, H. Yu, Y. Shi, X. Mou, M.K. Kalra, Y. Zhang, L. Sun, G. Wang, Low-Dose CT Image Denoising Using a Generative Adversarial Network With Wasserstein Distance and Perceptual Loss, IEEE Trans Med Imaging, 37 (2018) 1348-1357.

[98] F. Pesapane, M. Codari, F. Sardanelli, Artificial intelligence in medical imaging: threat or opportunity? Radiologists again at the forefront of innovation in medicine, European Radiology Experimental, 2 (2018).

[99] A. Hosny, C. Parmar, J. Quackenbush, L.H. Schwartz, H.J.W.L. Aerts, Artificial intelligence in radiology, Nat Rev Cancer, 18 (2018) 500-510.

[100] G.D. Luker, K.E. Luker, Optical imaging: current applications and future directions, J Nucl Med, 49 (2008) 1-4.

[101] G. Choy, P. Choyke, S.K. Libutti, Current advances in molecular imaging: noninvasive in vivo bioluminescent and fluorescent optical imaging in cancer research, Mol Imaging, 2 (2003) 303-312.

[102] K. O'Neill, S.K. Lyons, W.M. Gallagher, K.M. Curran, A.T. Byrne, Bioluminescent imaging: a critical tool in pre-clinical oncology research, J Pathol, 220 (2010) 317-327.

[103] Y. Gao, K. Wang, Y. An, S. Jiang, H. Meng, J. Tian, Nonmodel-based bioluminescence tomography using a machine-learning reconstruction strategy, Optica, 5 (2018).

[104] W. van Elmpt, L. McDermott, S. Nijsten, M. Wendling, P. Lambin, B. Mijnheer, A literature review of electronic portal imaging for radiotherapy dosimetry, Radiother Oncol, 88 (2008) 289-309.

[105] W. Ngwa, H. Korideck, L. Chin, M. Makrigiorgos, R. Berbeco, SU-E-T-317: MOSFET Assessment of Radiation Dose Delivered to Mice Using the Small Animal Radiation Research Platform (SARRP), Medical Physics, 38 (2011) 3560-3560.

[106] L. Wack, W. Ngwa, E. Tryggestad, P. Tsiamas, R. Berbeco, S.K. Ng, J. Hesser, P. Zygmanski, High throughput film dosimetry in homogeneous and heterogeneous media for a small animal irradiator, Phys Med, 30 (2014) 36-46.

[107] P.V. Granton, M. Podesta, G. Landry, S. Nijsten, G. Bootsma, F. Verhaegen, A combined dose calculation and verification method for a small animal precision irradiator based on onboard imaging, Med Phys, 39 (2012) 4155-4166.

[108] A. Anvari, Y. Poirier, A. Sawant, Development and implementation of EPID-based quality assurance tests for the small animal radiation research platform (SARRP), Med Phys, 45 (2018) 3246-3257.

[109] A. Anvari, Y. Poirier, A. Sawant, Kilovoltage transit and exit dosimetry for a small animal image-guided radiotherapy system using built-in EPID, Med Phys, 45 (2018) 4642-4651.

[110] M. Prall, M. Durante, T. Berger, B. Przybyla, C. Graeff, P.M. Lang, C. LaTessa, L. Shestov, P. Simoniello, C. Danly, F. Mariam, F. Merrill, P. Nedrow, C. Wilde, D. Varentsov, High-energy proton imaging for biomedical applications, Sci Rep, 6 (2016) 27651.

[111] H. Paganetti, Relative biological effectiveness (RBE) values for proton beam therapy. Variations as a function of biological endpoint, dose, and linear energy transfer, Phys Med Biol, 59 (2014) R419-472.

[112] E. Fokas, G. Kraft, H. An, R. Engenhart-Cabillic, Ion beam radiobiology and cancer: time to update ourselves, Biochim Biophys Acta, 1796 (2009) 216-229.

[113] P.E. Borchardt, R.R. Yuan, M. Miederer, M.R. McDevitt, D.A. Scheinberg, Targeted Actinium-225 in Vivo Generators for Therapy of Ovarian Cancer, Cancer Research, 63 (2003) 5084-5090.

[114] M.R. McDevitt, G. Sgouros, R.D. Finn, J.L. Humm, J.G. Jurcic, S.M. Larson, D.A. Scheinberg, Radioimmunotherapy with alpha-emitting nuclides, Eur J Nucl Med, 25 (1998) 1341-1351.

[115] J.J. Orozco, T. Back, A. Kenoyer, E.R. Balkin, D.K. Hamlin, D.S. Wilbur, D.R. Fisher, S.L. Frayo, M.D. Hylarides, D.J. Green, A.K. Gopal, O.W. Press, J.M. Pagel, Anti-CD45 radioimmunotherapy using (211)At with bone marrow transplantation prolongs survival in a disseminated murine leukemia model, Blood, 121 (2013) 3759-3767.

[116] S.E. Gould, M.R. Junttila, F.J. de Sauvage, Translational value of mouse models in oncology drug development, Nature Medicine, 21 (2015) 431.

[117] B.F. Koontz, F. Verhaegen, D. De Ruysscher, Tumour and normal tissue radiobiology in mouse models: how close are mice to mini-humans?, Br J Radiol, 90 (2017) 20160441.

7